Elsevier Editorial System(tm) for Journal of Solid State Chemistry
Manuscript Draft

Corresponding Author: Dr Rosalind Gummow, PhD

Corresponding Author's Institution: James Cook University

First Author: Rosalind Gummow, PhD

Order of Authors: Rosalind Gummow, PhD; Neeraj Sharma, PhD; Vanessa K Peterson, PhD; Yinghe He, PhD

Abstract: The crystal structure of the Pmnb polymorph of Li2MnSiO4 (prepared by solid-state synthesis in argon at 900^0C) is characterized by Rietveld refinement of structural models using high resolution synchrotron X-ray and neutron powder diffraction data. The crystal structure is confirmed to be isostructural with Li2CdSiO4 with lattice parameters a = 6.30694(3), b =10.75355(4) and c = 5.00863(2) Å, which are in good agreement with previously published data. No evidence was found for mixed lithium/manganese sites. Testing of the material as a cathode in a lithium cell shows that 1.3 lithium ions per formula unit can be extracted on the first charge cycle but very little lithium can be re-inserted. These results are compared with those of other phase-pure Li2MnSiO4 polymorphs.

School of Engineering and Physical Sciences
James Cook University
Townsville
Queensland, 4811
Australia
30/11/2011

The Editor
Journal of Solid State Chemistry

Dear H.-C. zur Loye,

Revised Manuscript Submission

Thank you for the opportunity to submit a revised manuscript of the publication : **Crystal Chemistry of the Pmnb polymorph of Li$_2$MnSiO$_4$** for consideration for publication in your high-quality journal.   We thank the reviewer for his/her helpful and constructive suggestions. We have modified the document in accordance with the reviewer's suggestions and include the revised manuscript and rebuttal document for your consideration.

We hope you will find this revised submission suitable for publication in your journal. Your assistance in this matter is appreciated.

Yours sincerely

R J Gummow

Response to reviewers

Ms. No.: JSSC-11-1077
Title: Crystal Chemistry of the Pmnb polymorph of Li2MnSiO4
Corresponding Author: Dr Rosalind Gummow
Authors: Rosalind J Gummow, PhD; Neeraj Sharma, PhD; Vanessa K. Peterson and Yinghe He

We would like to thank the reviewer for his/her helpful and constructive comments and address the points raised below:

1) I think the manuscript as presented is too long. This is a relatively simply story and the resulting paper should aim for brevity.
   The authors agree that the findings of the study should be presented as briefly as possible while still retaining clarity. We have modified the document, as suggested by the reviewer, by moving the infra-red data to the supplementary data and modifying the text as suggested.

2) The section on the top of page 10 on combined refinements is un-necessary save the first sentence should appear in the experimental section.
   The section at the top of page 10, save the first sentence, has been moved to the experimental section (pg 6), as suggested.

3) The discussion of the BVS on the bottom on page 11 is circular -the BVS is smaller than expected reflecting the longer than expected bond distances.
   The circular discussion on the BVS has been modified as recommended.

4) The FTIR section adds nothing to the paper - the spectra could go in supplementary material and the discussion on page 13 removed.
   The FTIR spectrum has been included in the supplementary information and the discussion has been deleted.

5) The isotopic sensitivity of NPD affords a higher sensitivity for elements such as lithium and oxygen than XRPD". WHAT? NPD is considerably less sensitive for all elements than XRD - what they possibly mean is neutrons are relatively more sensitive to Li than Mn compared to XRD. However this is a difficult argument - because the neutron scattering length of Mn is negative it is not immediately obvious to me how this translates into precision of the structural refinement. As an aside given Mn is the heaviest atom present good synchrotron data is capable of providing equivalent precision and accuracy for the anion positions as neutrons. I suggest removing the offending sentence.
   The sentence has been removed.

6) Scientifically I have one significant concern. What causes the distortion of the MnO4 tetrahedra (and don't say the BVS). The CdO4 tetrahedra in Li¬2¬CdSiO4 (Riekel Acta Cryst. (1977). B33, 2656-2657) is much less distorted than the MnO4 tetrahedra described here. If anisotropic ADP are utilised in refinement is there any evidence for unusual displacements of the Mn. This may afford a clue to the stability of the material.
   The authors thank the reviewer for pointing out the distortion of the manganese tetrahedra. Distortion of tetrahedra in silicates has, in some cases, been explained by face-sharing tetrahedra e.g in some Li_2FeSiO_4 phases. However, in this case, only the Li tetrahedra share faces so this cannot explain the distortion in the Mn tetrahedra. If we compare the data of Riekel for Li_2CdSiO_4 that the reviewer refers to, the Cd tetrahedra are also quite distorted (the O(2)-Cd(1)-O(2) angle is 126.1 degrees compared to O(2)-Mn-O(2) of 125.97). It seems, therefore, that the degree of distortion is similar for the two compounds. A comment to this effect has been included on page 12. The origin of the distortion is not known at this stage. We plan to do future in-situ studies of the crystal structure of this material with Li extraction which should indicate precisely what changes occur.

Crystal Chemistry of the *Pmnb* polymorph of Li$_2$MnSiO$_4$

R.J. Gummow[a]*, N. Sharma[b], V.K. Peterson[b] and Y. He[a]

a. School of Engineering and Physical Sciences, James Cook University, Douglas, Queensland, 4811, Australia

b. The Bragg Institute, Australian Nuclear Science and Technology Organization, Locked Bag 2001, Kirrawee DC NSW 2232, Australia

*corresponding author Email address: rosalind.gummow@jcu.edu.au

Tel: +61 7 47816223 Fax: +61 7 47816788

Crystal Chemistry of the *Pmnb* polymorph of Li$_2$MnSiO$_4$

R.J. Gummow[a]*, N. Sharma[b], V.K. Peterson[b] and Y. He[a]

a. School of Engineering and Physical Sciences, James Cook University, Douglas,

Queensland, 4811, Australia

b. The Bragg Institute, Australian Nuclear Science and Technology Organization, Locked

Bag 2001, Kirrawee DC NSW 2232, Australia

*corresponding author Email address: rosalind.gummow@jcu.edu.au

Tel: +61 7 47816223 Fax: +61 7 47816788

Abstract

The crystal structure of the *Pmnb* polymorph of Li_2MnSiO_4 (prepared by solid-state synthesis in argon at 900 ^oC) is characterized by Rietveld refinement of structural models using high resolution synchrotron X-ray and neutron powder diffraction data. The crystal structure is confirmed to be isostructural with Li_2CdSiO_4 with lattice parameters $a = 6.30694(3)$, $b = 10.75355(4)$, and $c = 5.00863(2)$ Å, which are in good agreement with previously published data. No evidence was found for mixed lithium/manganese sites. Testing of the material as a cathode in a lithium cell shows that 1.3 lithium ions per formula unit can be extracted on the first charge cycle but very little lithium can be re-inserted. These results are compared with those of other phase-pure Li_2MnSiO_4 polymorphs.

1. Introduction

Over the last ten years, the emphasis in lithium-ion battery development has shifted from small-scale portable applications to large-scale systems. These large-scale systems are required both for electric vehicles and as storage to compensate for the variable output of renewable-energy systems. Current lithium-ion battery chemistries cannot fully meet the demands of these applications in terms of cost as well as cycle- and calendar-life. Research to find new systems and to optimize existing systems is on-going [1-3].

Expensive raw materials are a major contributor to the cost of large-scale lithium ion batteries, with the cathode as the most expensive single component. To meet the market targets for the price of these batteries it is essential to develop low-cost cathode materials [4]. The lithium transition metal orthosilicates (Li_2MSiO_4 where $M=$ Fe, Co, or Mn), represent a new class of lithium-ion battery cathode and offer potential cost advantages because of the natural abundance of silica, iron, and manganese [5-9]. Li_2FeSiO_4 has shown promise as a cathode material [9, 10], but Li_2MnSiO_4 is even more attractive. For Li_2MnSiO_4, the possibility exists for the extraction of two lithium ions per formula unit at moderate voltages, resulting in a high theoretical capacity (> 300 mAhg^{-1} for the complete removal and re-insertion of two lithium ions per formula unit). Li_2MnSiO_4 has, however, so far failed to be developed as a cathode because of several limiting factors outlined below [10-14].

The practical application of Li_2MnSiO_4 as a cathode is limited by its low electronic conductivity of 5x10^{-16} Scm^{-1} at room temperature, increasing to 3x10^{-14} Scm^{-1} at 60 °C, which is 5-6 orders of magnitude smaller than that of the poorly conducting $LiFePO_4$ at room

temperature [5, 15]. Nanostructuring of particles and application of a conductive carbon

coating on particles are both strategies employed to overcome the problem of low

conductivity in LiFePO$_4$ [16]. Carbon addition is also common practice in the synthesis of

Li$_2$MnSiO$_4$, resulting in composite materials with both enhanced electronic properties and

improved electrochemical performance compared to carbon-free samples [10-14, 17-19].

Despite efforts aimed at improving the electronic properties of Li$_2$MnSiO$_4$ by carbon

addition, all reported cycling data for Li$_2$MnSiO$_4$ have shown a steady decrease in capacity

with cycling. This is in contrast to cycling data for Li$_2$FeSiO$_4$, which maintains a stable

discharge capacity for multiple cycles [10, 20]. The failure of Li$_2$MnSiO$_4$ to cycle reversibly

has been attributed to structural collapse and amorphization upon lithium extraction [5, 21].

Detailed studies of the partially delithiated $Pmn2_1$ polymorph of Li$_2$MnSiO$_4$ using in-situ

XRD, TEM, and NMR have clearly indicated that partial amorphization of the Li$_2$MnSiO$_4$

structure occurs upon lithium extraction [22]. This raises the question as to whether this

amorphization is common to all polymorphs of Li$_2$MnSiO$_4$, or whether other polymorphs

perform differently when lithium is extracted.

Phase-pure samples of Li$_2$MnSiO$_4$ are difficult to prepare as the lithium transition metal

orthosilicates exhibit several different polymorphs when synthesized under moderate

conditions [8, 21, 23]. Arroyo de-Dompablo *et al.* [21] have reported that there are, at least,

three polymorphs of Li$_2$MnSiO$_4$ that form at ambient pressure - two orthorhombic forms

(adopting $Pmn2_1$ and $Pmnb$ space group symmetries) and a monoclinic form (adopting $P2_1/n$

space group symmetry). Both the low-temperature orthorhombic forms are more stable than

the monoclinic form, which can only be prepared above 900 ºC [24, 25]. The crystal

structures of Li$_2$MnSiO$_4$ belong to the group of tetrahedral oxides with all cations

tetrahedrally coordinated between distorted close-packed layers of oxygen atoms. The

polymorphs can be related to the different polymorphic forms of Li_3PO_4 and differ in the orientation and connectivity of the cation tetrahedra. Structural refinements of the $Pmn2_1$ and the $P2_1/n$ forms have been reported [6, 25]. In contrast, while X-ray diffraction data has been collected [21, 24], no in-depth structural analysis of the $Pmnb$ form has been reported to date. All synthesized samples of this polymorph have included significant impurities, such as Li_2SiO_3, Mn_2SiO_4, MnO, and the $P2_1/n$ polymorph [21, 24], preventing accurate structural determination of the $Pmnb$ form of Li_2MnSiO_4.

In this study we report the facile synthesis by solid-state techniques of essentially single-phase samples of the $Pmnb$ polymorph of Li_2MnSiO_4 and its crystal-structure determined using synchrotron X-ray powder diffraction (SXRPD) and neutron powder diffraction (NPD) data. Morphological and FTIR spectroscopy data, as well as galvanostatic cell-cycling performance in lithium cells, are also reported.

2.   Experimental

Samples of Li_2MnSiO_4 were synthesized by a solid-state route. Stoichiometric quantities of LiOH (Sigma-Aldrich, > 98%), $MnCO_3$ (Sigma-Aldrich, > 99.9%), SiO_2 (fumed, Sigma-Aldrich, 0.007 μm), together with 20 mol. % adipic acid, were milled with dry hexane in a vibratory ball mill for 1 hour. The mixed powders were heated at 1 ℃ per min to 450 ℃ for 10 hours under dynamic vacuum to decompose the precursors. The resulting fine, dark brown powder was ground in a mortar and pestle and then heated to 700 ℃ for 10 h in argon in a tube furnace to prevent oxidation of the Mn^{2+}. To complete the reaction, the sample was

5

heated to 900 ℃ for a further 10 hours in argon and allowed to cool to room temperature in the furnace. Sample powders were stored in an argon glovebox.

The synthesized powders were initially characterized by conventional X-ray powder diffraction (XRPD) using a Siemens D5000 and a Panalytical X'pert Pro X-ray diffractometer with Cu-K$_\alpha$ radiation. Additional high-resolution SXRPD data were collected on the Powder Diffraction beamline (10-BM-1) [26] at the Australian Synchrotron using a wavelength (λ) of 0.82599(2) Å, determined using the NIST 660a LaB$_6$ standard reference material. Powder samples were packed and sealed in 0.5 mm glass capillaries in an argon glovebox and data were collected for 6 minutes at ambient temperature using Debye-Scherrer geometry. Neutron powder diffraction (NPD) data were collected using the high-resolution powder diffractometer, ECHIDNA, at the Open Pool Australian Light-water (OPAL) reactor facility at the Australian Nuclear Science and Technology Organisation (ANSTO) [27]. Data were collected at $\lambda = 1.62285(2)$ Å for 9 hours in the 2θ range $14 \leq 2\theta \leq 154°$, with the wavelength determined using the NIST Al$_2$O$_3$ SRM 676. Samples were sealed in 6 mm diameter vanadium cans with indium gaskets in an argon glovebox and data were collected at ambient temperature. Rietveld refinements were carried out using the GSAS [28] software suite with the EXPGUI [29] software interface. The SXRD and NPD datasets were initially refined separately. Finally, a combined refinement of both the SXRD and NPD datasets was performed. Atomic parameters for the elements in the starting model of the combined refinement were derived from the single dataset refinements, using the results from the dataset that provided the better contrast for each element relative to others. Using this approach, parameters for manganese and silicon were taken from the SXRPD data-derived

model and parameters for the lithium and oxygen were taken from the NPD data-derived model.

Particle morphology was determined by analysis of scanning-electron microscope images obtained with a JEOL JSM-5410LV instrument. Lithium and manganese content was determined by inductively coupled plasma-atomic emission spectrometry (ICP-AES) using a Varian Liberty Series II instrument. Samples were digested in hydrofluoric acid prior to analysis. Silicon is lost in the digestion process and therefore could not be analysed.

Energy-dispersive spectroscopy (EDS) was performed on carbon-coated powder samples using an electron-probe micro analyser (EPMA) to determine the manganese to silicon ratio of the product phases. Averages were taken of six measurements at different positions in the sample. Elements with low atomic mass cannot accurately be analyzed on this instrument so it was not possible to accurately determine lithium or oxygen contents.

FTIR spectra were collected on powder samples in transmission mode between 700 and 1400 cm^{-1} using the diamond ATR on a Perkin-Elmer FTIR spectrometer (see Supporting Information).

To prepare electrodes for electrochemical characterization the sample powder was ball-milled with Super C-65 carbon (Timcal) in a vibratory ball-mill for 1 hour. The resulting powder was mixed with polyvinylidene difluoride (PVDF, Sigma-Aldrich) dissolved in n-methyl pyrrolidenone (NMP, anhydrous, 99.5%, Sigma-Aldrich) in a ratio of 74:13:13. Cathodes

7

were formed by coating the resulting slurry onto aluminium foil current collectors, followed by drying in vacuum for 10 hours at 120 °C and pressing with a hydraulic press to 15 MPa. Typical cathode masses were 1-2 mg with a surface area of 1.2 cm^2. Swagelok-type electrochemical test-cells were assembled in an argon glovebox. The electrolyte used was a solution of lithium hexafluorophosphate (battery grade, > 99.9%, Aldrich) in a 1:1 mixture by volume of ethylene carbonate and dimethyl carbonate (99%, Sigma-Aldrich). The anode consisted of a 12 mm diameter disc of 0.7 mm thick lithium metal foil. The anode and cathode were separated by two discs of microporous polypropylene separator film (Celgard) saturated with the electrolyte solution. Assembled cells were cycled galvanostatically using a battery analyzer (MTI Corporation).

3.   Results and Discussion

3.1   *Structural determination*

XRPD data for the samples formed at 700 ºC and 900 ºC are shown in Fig. 1b and c, respectively, together with a simulated XRPD pattern of the *Pmn*2$_1$ form of Li$_2$MnSiO$_4$ using the structural model of Dominko *et al* [6] (Fig.1a). We speculate that the presence of the carbon-containing adipic acid in the reaction mixture inhibits the formation of Li$_2$MnSiO$_4$ at 700 ºC in argon; after 10 hours peaks attributed to both Li$_2$SiO$_3$ and MnO remain (Fig. 1b). The disappearance of these impurity peaks on further heating to 900 ºC for 10 hours (Fig. 1 c) indicates that the reaction approaches completion at this temperature. The product was a dark grey colour and the relatively sharp diffraction peaks indicate that a crystalline product formed at the relatively high temperature of 900 ºC. Notably, the XRPD data of the material obtained after heating to 900 ºC (Fig. 1c) contains peaks that are not present in the *Pmn*2$_1$ model for Li$_2$MnSiO$_4$ (Fig. 1a), but conforms to the expected pattern for the *Pmnb* form as

8

described by Arroyo de-Dompablo *et al*. [21] and Mali *et al*. [24]. In the study of Belharouak *et al.* [11], it was reported that Li_2MnSiO_4 samples heated above 700 ºC contained Li_2SiO_3 and Mn_2SiO_4 impurities; 700 ºC was found to be the optimal temperature for the synthesis of Li_2MnSiO_4 with the *Pmn2₁* structure. In the present study heating the sample above 700 ºC does not result in the formation of impurities but leads to the formation of the phase-pure *Pmnb* form of Li_2MnSiO_4. This sample represents the purest *Pmnb* form of Li_2MnSiO_4 that has been reported, a material that has proved difficult to synthesize without significant impurities in the past, and the crystallographic structure was studied further using high resolution SXRPD and NPD.

The Li_2CdSiO_4 –type [30] structure proposed by Arroyo de-Dompablo *et al*. [21] and Mali *et al*. [24] for the *Pmnb* form of Li_2MnSiO_4, was used as a starting model with silicon, lithium, and manganese each occupying individual atomic sites without any cation mixing. No evidence was found for Li_2SiO_3 and Mn_2SiO_4 impurities or other polymorphs of Li_2MnSiO_4 in the sample. A few small reflections in the SXRPD data were accounted for with the inclusion of MnO as a minor impurity phase (< 1 %). Permutations of the ideal model, such as lithium-ion vacancies and cation mixing on lithium and/or manganese sites, were tested but were not found to describe the data (i.e. did not result in statistically significant improvements of the fit of the model to the data).

The structural model and permutations tested against the SXRPD data were again tested against the NPD data. The Lobanov and Alte da Veiga absorption correction [28, 31] was applied in the Rietveld model to account for absorption of neutrons by the sample, which was significant as a consequence of the relatively large neutron absorption cross-section of

9

lithium (63.632 barn at $\lambda = 1.62285(2)$ Å) [32]. The ideal model, containing no cation

mixing, proved to be the best fit to the NPD data. Model permutations such as lithium-ion

vacancies and mixed sites were tested and again were found not to describe the data.

Rietveld refinement of the structural model was performed using both SXRPD and NPD

datasets simultaneously, referred to as a combined refinement [33-35]. The refined lattice

parameters obtained from the combined refinement are $a = 6.30694(3)$ Å, $b = 10.75355(4)$ Å,

and $c = 5.00863(2)$ Å, which are closer to the lattice constants reported by Arroyo-de

Dompablo *et al.* of $a = 6.30814(13)$ Å, $b = 10.75946(22)$ Å and $c=5.00909(10)$ Å for the

Pmnb phase [21], than to those reported by Mali *et al* of $a = 6.3148(1)$ Å, $b = 10.7742(5)$ Å,

and $c = 5.0138(2)$ Å [24]. The manganese to silicon ratio of the sample, analysed using EDS,

was found to be 0.9(1):1.0 and the lithium to manganese ratio obtained from the ICP-AAS

analysis was 2:0.95(3). These results are in agreement with the nominal stoichiometry of

Li_2MnSiO_4. The final structural model (Table 1), with lithium, manganese, and silicon ions

fully occupying individual tetrahedral sites and no cation mixing is obtained from combined

refinements with 45 variables with figures of merit that include the profile factor (R_p) =

2.74%, the weighted-profile factor (wR_p) = 3.70%, and the goodness-of-fit term (χ^2) = 1.86,

and Bragg *R*-factors ($R_F{}^2$) of 9.31% and 8.73% for the NPD and SXRPD reflection lists,

respectively (Fig. 2a, b and 3). Bond-valence sums (BVS) [35], bond lengths, and bond

angles for the refined structural model were physically reasonable (Tables 1 and 2).

The structural model obtained in this study confirms the proposed Li_2CdSiO_4-type structure

for the *Pmnb* polymorph of Li_2MnSiO_4 (Fig. 4a) [21, 24]. The structure features two-

dimensional "layers" of alternating, corner-sharing silicon and manganese tetrahedra in the

(010) plane linked along the [010] direction by double-chains of lithium tetrahedra. The SiO_4 and MnO_4 tetrahedra share corners with the lithium tetrahedra. The two chains of Li tetrahedra share faces in the [010] direction. There is no face-sharing between the MnO_4 tetrahedra and either the SiO_4 or LiO_4 tetrahedra. It should be noted that this structure is different from that of the recently reported *Pmnb* polymorph of Li_2FeSiO_4 formed at 900 °C, in which edge-sharing of the LiO_4 and FeO_4/CoO_4 tetrahedra occurs [36, 37].

The average Si-O and Li-O bond lengths are 1.644(3) Å and 1.961(9) Å, respectively (Table 2). These bond lengths are in agreement with the expected distances of 1.64 Å and 1.97 Å for Si-O and Li-O, respectively, based on their expected ionic sizes in tetrahedral coordination [38, 39]. The average Mn-O bond length of 2.079(3) Å is significantly larger than the expected bond length of 2.04 Å, based on ionic size, but is in reasonable agreement with the average value of 2.0910 Å predicted by the computational model of Arroyo *et al*. [21] for the *Pmnb* structure. This indicates that the manganese tetrahedra are distorted, which is confirmed by the large distribution of O-Mn-O bond angles. This finding is in agreement with the published data for Li_2CdSiO_4 which shows distorted Cd tetrahedra [30].

BVS (Table 1) show that all atoms (with the exception of lithium) are underbonded. In particular, the BVS sum for manganese is 15.5% less than the expected value, which is consistent with the distorted manganese tetrahedra (Table 2). The BVS for the other atoms, although less than the expected values, are within the acceptable range of values considering the approximate nature of BVS calculations.

Complete delithiation of Li_2MnSiO_4 with *Pmnb* symmetry (Fig. 4b) would result in $MnSiO_4$ layers disconnected from each other, causing lattice expansion along the y-direction as a consequence of the electrostatic repulsion of the oxygen anions in adjacent layers. This delithiated state is therefore unlikely to occur in practice. It is more likely that delithiation of Li_2MnSiO_4 with *Pmnb* symmetry would result in a lattice re-arrangement (as demonstrated for Li_2FeSiO_4) or structural collapse and amorphization (as found for the *Pmn*2_1 polymorph of Li_2MnSiO_4) [5, 13, 22, 40]. A driver for structural change is the instability of Mn^{3+} and Mn^{4+} in tetrahedral coordination. Mn^{3+} is typically found in distorted octahedral or square-pyramidal coordination while Mn^{4+} is usually found in octahedral coordination. This implies that oxidizing Mn^{2+} while maintaining tetrahedral coordination is likely to be difficult [25]. The presence of Mn^{3+} cations in delithiated Li_2MnSiO_4 may also result in a dynamic Jahn-Teller distortion of the lattice, which has been shown to be a significant factor in the capacity fade of other Mn^{3+}-containing cathode materials such as $LiMn_2O_4$ spinels [41].

3.2   *Morphology*

SEM analysis of the material shows that smaller particles are sintered together to form larger, irregular agglomerates of up to 50 µm, consistent with the relatively high temperature of synthesis (900 ℃, Fig. 5). Despite the presence of the carbonaceous additive (adipic acid), the sintering process is not inhibited at this high temperature.

3.3   *Electrochemistry*

Fig. 6 shows the galvanostatic charge and discharge curves for the first cycle for a Li/Li$_2$MnSiO$_4$ (*Pmnb* polymorph) cell at ambient temperature with a current rate of 20 mAg^{-1} and voltage limits of 4.9 and 2.5 V, respectively. The first charge cycle shows a steady increase in voltage with charge and a capacity of 230 mAhg^{-1}, corresponding to the extraction of 1.3 lithium per formula unit. Lithium cannot be re-inserted in large quantities on the subsequent discharge (20 mAhg^{-1}, corresponding to 0.1 lithium per formula unit).

The poor electrochemical performance may be ascribed to two factors. Firstly, it should be noted that the morphology of this sample (Fig.5), prepared by solid state synthesis, is not optimal for electrochemical performance. Large, poorly-conducting particles result in large polarization and it is possible that some of the capacity observed on charge can be attributed to irreversible reactions, for example, electrolyte decomposition, occurring at the high voltages reached and not exclusively to lithium extraction. Since the *Pmnb* polymorph of Li$_2$MnSiO$_4$ can be readily formed in the solid state at 900 ^{o}C, alternative synthesis routes e.g. sol-gel or hydrothermal synthesis that typically generate fine particles with a carbon coating, are also expected to yield this polymorph at calcination temperatures above 700 ^{o}C. Fine, carbon-coated powders would show reduced polarization on charge enabling the extraction of lithium at lower voltages and preventing unwanted side-reactions. Secondly, it is likely that, as in the case of the *Pmn*2$_1$ polymorph, the extraction of lithium during the first charge cycle results in a structural re-arrangement or amorphization of the lattice which limits lithium re-insertion on the subsequent discharge cycle [5, 13, 22].

4.   Conclusion

In this study we have prepared the *Pmnb* polymorph of Li$_2$MnSiO$_4$ without significant impurities. Rietveld refinement of a structural model using a combination of high resolution

SXRPD and NPD data shows that the sample is isostructural with Li_2CdSiO_4 with $a = 6.30694(3)$ Å, $b = 10.75355(4)$ Å, and $c = 5.00863(2)$ Å, confirming the previously proposed structure [21, 24]. Bond lengths, angles, and BVS from this model are physically realistic, where the manganese tetrahedra are found to be distorted. Electrochemical results show poor galvanostatic cycling performance. Alternative synthesis routes aimed at improving the electrochemical performance of this polymorph will be explored in future work.

.

References

[1]   Z.G. Yang, J. Liu, S. Baskaran, C.H. Imhoff, J.D. Holladay, J.O.M. 62 (2010) 14-23.

[2]   T. Xu, W. Wang, M.L. Gordin, D.H. Wang, D.W. Choi, J.O.M. 62 (2010) 24-30.

[3]   A. Manthiram, J. Phys. Chem. 2 (2011) 176-184.

[4]   C. Daniel, J.O.M. 60 (2008) 43-48.

[5]   R. Dominko, J. Power Sources 184 (2008) 462-468.

[6]   R. Dominko, M. Bele, M. Gaberscek, A. Meden, M. Remskar, J. Jamnik, Electrochem. Commun. 8 (2006) 217-222.

[7]   R. Dominko, M. Bele, A. Kokalj, M. Gaberscek, J. Jamnik, J.Power Sources 174 (2007) 457-461.

[8]   C. Lyness, B. Delobel, A.R. Armstrong, P.G. Bruce, Chem. Commun. (2007) 4890-4892.

[9]   A. Nyten, A. Abouimrane, M. Armand, T. Gustafsson, J.O. Thomas, Electrochem. Commun. 7 (2005) 156-160.

[10]   C. Deng, S. Zhang, B.L. Fu, S.Y. Yang, L. Ma, Mater. Chem.Phys. 120 (2010) 14-17.

[11]   I. Belharouak, A. Abouimrane, K. Amine, J. Phys. Chem. C 113 (2009) 20733-20737.

[12]   W.G. Liu, Y.H. Xu, R. Yang, J. Alloys Compds. 480 (2009) L1-L4.

[13]   W.G. Liu, Y.H. Xu, R. Yang, Rare Metals 29 (2010) 511-514.

[14]   W.G. Liu, Y.H. Xu, R. Yang, M. Hojamberdiev, Z.B. Zhou, J. Inorg. Mater. 25 (2010) 327-331.

[15]   V. Srinivasan, J. Newman, J. Electrochem. Soc. 151 (2004) A1517-A1529.

[16]   J.D. Wilcox, M.M. Doeff, M. Marcinek, R. Kostecki, J. Electrochem. Soc. 154 (2007) A389-A395.

[17]   A. Manthiram, T. Muraliganth, K.R. Stroukoff, Chem. Mater. 22 (2010) 5754-5761.

[18]   V. Aravindan, K. Karthikeyan, S. Ravi, S. Amaresh, W.S. Kim, Y.S. Lee, J. Mater. Chem. 20 (2010) 7340-7343.

[19]   K. Karthikeyan, V. Aravindan, S.B. Lee, I.C. Jang, H.H. Lim, G.J. Park, M. Yoshio, Y.S. Lee, J. Power Sources 195 (2010) 3761-3764.

[20]   D. Lv, W. Wen, X. Huang, J. Bai, J. Mi, S. Wu, Y. Yang, J. Mater. Chem. 21 (2011) 9506-9512.

[21]   M.E. Arroyo-DeDompablo, R. Dominko, J.M. Gallardo-Amores, L. Dupont, G. Mali, H. Ehrenberg, J. Jamnik, E. Moran, Chem. Mater. 20 (2008) 5574-5584.

[22]   A. Kokalj, R. Dominko, G. Mali, A. Meden, M. Gaberscek, J. Jamnik, Chem. Mater. 19 (2007) 3633-3640.

[23]   A.R. Armstrong, C. Lyness, M. Menetrier, P.G. Bruce, Chem. Mater. 22 (2010) 1892-1900.

[24]   G. Mali, A. Meden, R. Dominko, Chem. Commun. 46 (2010) 3306-3308.

[25]   V.V. Politaev, A.A. Petrenko, V.B. Nalbandyan, B.S. Medvedev, E.S. Shvetsova, J. Solid State Chem. 180 (2007) 1045-1050.

[26]   K.S. Wallwork, B.J. Kennedy, D. Wang, AIP Conference Proceedings (2007) 879.

[27]   K.D. Liss, B. Hunter, M. Hagen, T. Noakes, S. Kennedy, Physica B 385-86 (2006) 1010-1012.

[28]   A.C. Larson, R.B.V. Dreele, Los Alamos National Laboratory Report LAUR (1994) 86-748.

[29]   B.H. Toby, J. Appl. Crystallogr. 34 (2001) 210-213.

[30]   C. Riekel, Acta Crystallogr. B 33 (1977) 2656-2657.

[31]   N.N. Lobanov, L.A.d. Veiga, Sixth European Powder Diffraction Conference August 22-25 (1998).

[32]   V.F. Sears, Neutron News 3 (1992) 29.

[33]   N. Sharma, R.L. Withers, K.S. Knight, C.D. Ling, J. Solid State Chem. 182 (2009)

        2468-2474.

[34]   N. Sharma, R.B. Macquart, M.M. Avdeev, M. Christensen, G.I. McIntyre, Y.-S.

        Chen, C.D. Ling, Acta Crystallogr. B 66 (2010) 165-172.

[35]   R.J. Gummow, N. Sharma, V.K. Peterson, Y. He, J. Power Sources (2011)

        doi:10.1016/j.jpowsour.2011.09.013.

[36]   A. Boulineau, C. Sirisopanaporn, R. Dominko, A.R. Armstrong, P.G. Bruce, C.

        Masquelier, Dalton Trans. 39 (2010) 6310-6316.

[37]   C. Sirisopanaporn, A. Boulineau, D. Hanzel, R. Dominko, B. Budic, A.R. Armstrong,

        P.G. Bruce, C. Masquelier, Inorg. Chem. 49 (2010) 7446-7451.

[38]   R.D. Shannon and C.T. Prewitt, J. Inorg. Nucl. Chem. 32 (1970) 1427-1441.

[39]   R.D. Shannon, C.T. Prewitt, Acta Crystallogr. B 25 (1969) 925.

[40]   A.R. Armstrong, N. Kuganathan, M.S. Islam, P.G. Bruce, J. Am. Chem. Soc. 133

        (2011) 13031-13035.

[41]   R.J. Gummow, A. De Kock, M.M. Thackeray, Solid State Ionics 69 (1994) 59-67.

Crystal Chemistry of the *Pmnb* polymorph of Li$_2$MnSiO$_4$

R.J. Gummow^{a}*, N. Sharma^{b}, V.K. Peterson^{b} and Y. He^{a}

a. School of Engineering and Physical Sciences, James Cook University, Douglas, Queensland, 4811, Australia

b. The Bragg Institute, Australian Nuclear Science and Technology Organization, Locked Bag 2001, Kirrawee DC NSW 2232, Australia

*corresponding author Email address: rosalind.gummow@jcu.edu.au

Tel: +61 7 47816223 Fax: +61 7 47816788

Abstract

The crystal structure of the *Pmnb* polymorph of Li_2MnSiO_4 (prepared by solid-state synthesis in argon at 900 ^oC) is characterized by Rietveld refinement of structural models using high resolution synchrotron X-ray and neutron powder diffraction data. The crystal structure is confirmed to be isostructural with Li_2CdSiO_4 with lattice parameters $a = 6.30694(3)$, $b = 10.75355(4)$, and $c = 5.00863(2)$ Å, which are in good agreement with previously published data. No evidence was found for mixed lithium/manganese sites. Testing of the material as a cathode in a lithium cell shows that 1.3 lithium ions per formula unit can be extracted on the first charge cycle but very little lithium can be re-inserted. These results are compared with those of other phase-pure Li_2MnSiO_4 polymorphs.

1. Introduction

Over the last ten years, the emphasis in lithium-ion battery development has shifted from small-scale portable applications to large-scale systems. These large-scale systems are required both for electric vehicles and as storage to compensate for the variable output of renewable-energy systems. Current lithium-ion battery chemistries cannot fully meet the demands of these applications in terms of cost as well as cycle- and calendar-life. Research to find new systems and to optimize existing systems is on-going [1-3].

Expensive raw materials are a major contributor to the cost of large-scale lithium ion batteries, with the cathode as the most expensive single component. To meet the market targets for the price of these batteries it is essential to develop low-cost cathode materials [4]. The lithium transition metal orthosilicates (Li_2MSiO_4 where $M=$ Fe, Co, or Mn), represent a new class of lithium-ion battery cathode and offer potential cost advantages because of the natural abundance of silica, iron, and manganese [5-9]. Li_2FeSiO_4 has shown promise as a cathode material [9, 10], but Li_2MnSiO_4 is even more attractive. For Li_2MnSiO_4, the possibility exists for the extraction of two lithium ions per formula unit at moderate voltages, resulting in a high theoretical capacity (> 300 mAhg^{-1} for the complete removal and re-insertion of two lithium ions per formula unit). Li_2MnSiO_4 has, however, so far failed to be developed as a cathode because of several limiting factors outlined below [10-14].

The practical application of Li_2MnSiO_4 as a cathode is limited by its low electronic conductivity of $5x10^{-16}$ Scm^{-1} at room temperature, increasing to $3x10^{-14}$ Scm^{-1} at 60 °C, which is 5-6 orders of magnitude smaller than that of the poorly conducting $LiFePO_4$ at room

temperature [5, 15]. Nanostructuring of particles and application of a conductive carbon

coating on particles are both strategies employed to overcome the problem of low

conductivity in $LiFePO_4$ [16]. Carbon addition is also common practice in the synthesis of

Li_2MnSiO_4, resulting in composite materials with both enhanced electronic properties and

improved electrochemical performance compared to carbon-free samples [10-14, 17-19].

Despite efforts aimed at improving the electronic properties of Li_2MnSiO_4 by carbon

addition, all reported cycling data for Li_2MnSiO_4 have shown a steady decrease in capacity

with cycling. This is in contrast to cycling data for Li_2FeSiO_4, which maintains a stable

discharge capacity for multiple cycles [10, 20]. The failure of Li_2MnSiO_4 to cycle reversibly

has been attributed to structural collapse and amorphization upon lithium extraction [5, 21].

Detailed studies of the partially delithiated *Pmn*2_1 polymorph of Li_2MnSiO_4 using in-situ

XRD, TEM, and NMR have clearly indicated that partial amorphization of the Li_2MnSiO_4

structure occurs upon lithium extraction [22]. This raises the question as to whether this

amorphization is common to all polymorphs of Li_2MnSiO_4, or whether other polymorphs

perform differently when lithium is extracted.

Phase-pure samples of Li_2MnSiO_4 are difficult to prepare as the lithium transition metal

orthosilicates exhibit several different polymorphs when synthesized under moderate

conditions [8, 21, 23]. Arroyo de-Dompablo *et al.* [21] have reported that there are, at least,

three polymorphs of Li_2MnSiO_4 that form at ambient pressure - two orthorhombic forms

(adopting *Pmn*2_1 and *Pmnb* space group symmetries) and a monoclinic form (adopting *P2*$_1$*/n*

space group symmetry). Both the low-temperature orthorhombic forms are more stable than

the monoclinic form, which can only be prepared above 900 ºC [24, 25]. The crystal

structures of Li_2MnSiO_4 belong to the group of tetrahedral oxides with all cations

tetrahedrally coordinated between distorted close-packed layers of oxygen atoms. The

4

polymorphs can be related to the different polymorphic forms of Li_3PO_4 and differ in the orientation and connectivity of the cation tetrahedra. Structural refinements of the $Pmn2_1$ and the $P2_1/n$ forms have been reported [6, 25]. In contrast, while X-ray diffraction data has been collected [21, 24], no in-depth structural analysis of the $Pmnb$ form has been reported to date. All synthesized samples of this polymorph have included significant impurities, such as Li_2SiO_3, Mn_2SiO_4, MnO, and the $P2_1/n$ polymorph [21, 24], preventing accurate structural determination of the $Pmnb$ form of Li_2MnSiO_4.

In this study we report the facile synthesis by solid-state techniques of essentially single-phase samples of the $Pmnb$ polymorph of Li_2MnSiO_4 and its crystal-structure determined using synchrotron X-ray powder diffraction (SXRPD) and neutron powder diffraction (NPD) data. Morphological and FTIR spectroscopy data, as well as galvanostatic cell-cycling performance in lithium cells, are also reported.

2. Experimental

Samples of Li_2MnSiO_4 were synthesized by a solid-state route. Stoichiometric quantities of LiOH (Sigma-Aldrich, > 98%), $MnCO_3$ (Sigma-Aldrich, > 99.9%), SiO_2 (fumed, Sigma-Aldrich, 0.007 μm), together with 20 mol. % adipic acid, were milled with dry hexane in a vibratory ball mill for 1 hour. The mixed powders were heated at 1 ℃ per min to 450 ℃ for 10 hours under dynamic vacuum to decompose the precursors. The resulting fine, dark brown powder was ground in a mortar and pestle and then heated to 700 ℃ for 10 h in argon in a tube furnace to prevent oxidation of the Mn^{2+}. To complete the reaction, the sample was

heated to 900 ºC for a further 10 hours in argon and allowed to cool to room temperature in the furnace. Sample powders were stored in an argon glovebox.

The synthesized powders were initially characterized by conventional X-ray powder diffraction (XRPD) using a Siemens D5000 and a Panalytical X'pert Pro X-ray diffractometer with Cu-K_α radiation. Additional high-resolution SXRPD data were collected on the Powder Diffraction beamline (10-BM-1) [26] at the Australian Synchrotron using a wavelength (λ) of 0.82599(2) Å, determined using the NIST 660a LaB$_6$ standard reference material. Powder samples were packed and sealed in 0.5 mm glass capillaries in an argon glovebox and data were collected for 6 minutes at ambient temperature using Debye-Scherrer geometry. Neutron powder diffraction (NPD) data were collected using the high-resolution powder diffractometer, ECHIDNA, at the Open Pool Australian Light-water (OPAL) reactor facility at the Australian Nuclear Science and Technology Organisation (ANSTO) [27]. Data were collected at λ = 1.62285(2) Å for 9 hours in the 2θ range 14 ≤ 2θ ≤ 154°, with the wavelength determined using the NIST Al$_2$O$_3$ SRM 676. Samples were sealed in 6 mm diameter vanadium cans with indium gaskets in an argon glovebox and data were collected at ambient temperature. Rietveld refinements were carried out using the GSAS [28] software suite with the EXPGUI [29] software interface. The SXRD and NPD datasets were initially refined separately. Finally, a combined refinement of both the SXRD and NPD datasets was performed. Atomic parameters for the elements in the starting model of the combined refinement were derived from the single dataset refinements, using the results from the dataset that provided the better contrast for each element relative to others. Using this approach, parameters for manganese and silicon were taken from the SXRPD data-derived

model and parameters for the lithium and oxygen were taken from the NPD data-derived model.

Particle morphology was determined by analysis of scanning-electron microscope images obtained with a JEOL JSM-5410LV instrument. Lithium and manganese content was determined by inductively coupled plasma-atomic emission spectrometry (ICP-AES) using a Varian Liberty Series II instrument. Samples were digested in hydrofluoric acid prior to analysis. Silicon is lost in the digestion process and therefore could not be analysed.

Energy-dispersive spectroscopy (EDS) was performed on carbon-coated powder samples using an electron-probe micro analyser (EPMA) to determine the manganese to silicon ratio of the product phases. Averages were taken of six measurements at different positions in the sample. Elements with low atomic mass cannot accurately be analyzed on this instrument so it was not possible to accurately determine lithium or oxygen contents.

FTIR spectra were collected on powder samples in transmission mode between 700 and 1400 cm^{-1} using the diamond ATR on a Perkin-Elmer FTIR spectrometer (see Supporting Information).

To prepare electrodes for electrochemical characterization the sample powder was ball-milled with Super C-65 carbon (Timcal) in a vibratory ball-mill for 1 hour. The resulting powder was mixed with polyvinylidene difluoride (PVDF, Sigma-Aldrich) dissolved in n-methyl pyrrolidenone (NMP, anhydrous, 99.5%, Sigma-Aldrich) in a ratio of 74:13:13. Cathodes

7

were formed by coating the resulting slurry onto aluminium foil current collectors, followed by drying in vacuum for 10 hours at 120 °C and pressing with a hydraulic press to 15 MPa. Typical cathode masses were 1-2 mg with a surface area of 1.2 cm^2. Swagelok-type electrochemical test-cells were assembled in an argon glovebox. The electrolyte used was a solution of lithium hexafluorophosphate (battery grade, > 99.9%, Aldrich) in a 1:1 mixture by volume of ethylene carbonate and dimethyl carbonate (99%, Sigma-Aldrich). The anode consisted of a 12 mm diameter disc of 0.7 mm thick lithium metal foil. The anode and cathode were separated by two discs of microporous polypropylene separator film (Celgard) saturated with the electrolyte solution. Assembled cells were cycled galvanostatically using a battery analyzer (MTI Corporation).

3. Results and Discussion

3.1 Structural determination

XRPD data for the samples formed at 700 °C and 900 °C are shown in Fig. 1b and c, respectively, together with a simulated XRPD pattern of the *Pmn*2_1 form of Li$_2$MnSiO$_4$ using the structural model of Dominko *et al* [6] (Fig.1a). We speculate that the presence of the carbon-containing adipic acid in the reaction mixture inhibits the formation of Li$_2$MnSiO$_4$ at 700 °C in argon; after 10 hours peaks attributed to both Li$_2$SiO$_3$ and MnO remain (Fig. 1b). The disappearance of these impurity peaks on further heating to 900 °C for 10 hours (Fig. 1 c) indicates that the reaction approaches completion at this temperature. The product was a dark grey colour and the relatively sharp diffraction peaks indicate that a crystalline product formed at the relatively high temperature of 900 °C. Notably, the XRPD data of the material obtained after heating to 900 °C (Fig. 1c) contains peaks that are not present in the *Pmn*2_1 model for Li$_2$MnSiO$_4$ (Fig. 1a), but conforms to the expected pattern for the *Pmnb* form as

described by Arroyo de-Dompablo *et al*. [21] and Mali *et al*. [24]. In the study of Belharouak *et al.* [11], it was reported that Li_2MnSiO_4 samples heated above 700 ºC contained Li_2SiO_3 and Mn_2SiO_4 impurities; 700 ºC was found to be the optimal temperature for the synthesis of Li_2MnSiO_4 with the *Pmn*2_1 structure. In the present study heating the sample above 700 ºC does not result in the formation of impurities but leads to the formation of the phase-pure *Pmnb* form of Li_2MnSiO_4. This sample represents the purest *Pmnb* form of Li_2MnSiO_4 that has been reported, a material that has proved difficult to synthesize without significant impurities in the past, and the crystallographic structure was studied further using high resolution SXRPD and NPD.

The Li_2CdSiO_4–type [30] structure proposed by Arroyo de-Dompablo *et al*. [21] and Mali *et al*. [24] for the *Pmnb* form of Li_2MnSiO_4, was used as a starting model with silicon, lithium, and manganese each occupying individual atomic sites without any cation mixing. No evidence was found for Li_2SiO_3 and Mn_2SiO_4 impurities or other polymorphs of Li_2MnSiO_4 in the sample. A few small reflections in the SXRPD data were accounted for with the inclusion of MnO as a minor impurity phase (< 1 %). Permutations of the ideal model, such as lithium-ion vacancies and cation mixing on lithium and/or manganese sites, were tested but were not found to describe the data (i.e. did not result in statistically significant improvements of the fit of the model to the data).

The structural model and permutations tested against the SXRPD data were again tested against the NPD data. The Lobanov and Alte da Veiga absorption correction [28, 31] was applied in the Rietveld model to account for absorption of neutrons by the sample, which was significant as a consequence of the relatively large neutron absorption cross-section of

lithium (63.632 barn at λ = 1.62285(2) Å) [32]. The ideal model, containing no cation

mixing, proved to be the best fit to the NPD data. Model permutations such as lithium-ion

vacancies and mixed sites were tested and again were found not to describe the data.

Rietveld refinement of the structural model was performed using both SXRPD and NPD

datasets simultaneously, referred to as a combined refinement [33-35]. The refined lattice

parameters obtained from the combined refinement are a = 6.30694(3) Å, b = 10.75355(4) Å,

and c = 5.00863(2) Å, which are closer to the lattice constants reported by Arroyo-de

Dompablo *et al.* of a = 6.30814(13) Å, b = 10.75946(22) Å and c=5.00909(10) Å for the

Pmnb phase [21], than to those reported by Mali *et al* of a = 6.3148(1) Å, b = 10.7742(5) Å,

and c = 5.0138(2) Å [24]. The manganese to silicon ratio of the sample, analysed using EDS,

was found to be 0.9(1):1.0 and the lithium to manganese ratio obtained from the ICP-AAS

analysis was 2:0.95(3). These results are in agreement with the nominal stoichiometry of

Li_2MnSiO_4. The final structural model (Table 1), with lithium, manganese, and silicon ions

fully occupying individual tetrahedral sites and no cation mixing is obtained from combined

refinements with 45 variables with figures of merit that include the profile factor (R_p) =

2.74%, the weighted-profile factor (wR_p) = 3.70%, and the goodness-of-fit term (χ^2) = 1.86,

and Bragg R-factors (R_F^2) of 9.31% and 8.73% for the NPD and SXRPD reflection lists,

respectively (Fig. 2a, b and 3). Bond-valence sums (BVS) [35], bond lengths, and bond

angles for the refined structural model were physically reasonable (Tables 1 and 2).

The structural model obtained in this study confirms the proposed Li_2CdSiO_4-type structure

for the *Pmnb* polymorph of Li_2MnSiO_4 (Fig. 4a) [21, 24]. The structure features two-

dimensional "layers" of alternating, corner-sharing silicon and manganese tetrahedra in the

(010) plane linked along the [010] direction by double-chains of lithium tetrahedra. The SiO_4 and MnO_4 tetrahedra share corners with the lithium tetrahedra. The two chains of Li tetrahedra share faces in the [010] direction. There is no face-sharing between the MnO_4 tetrahedra and either the SiO_4 or LiO_4 tetrahedra. It should be noted that this structure is different from that of the recently reported *Pmnb* polymorph of Li_2FeSiO_4 formed at 900 ºC, in which edge-sharing of the LiO_4 and FeO_4/CoO_4 tetrahedra occurs [36, 37].

The average Si-O and Li-O bond lengths are 1.644(3) Å and 1.961(9) Å, respectively (Table 2). These bond lengths are in agreement with the expected distances of 1.64 Å and 1.97 Å for Si-O and Li-O, respectively, based on their expected ionic sizes in tetrahedral coordination [38, 39]. The average Mn-O bond length of 2.079(3) Å is significantly larger than the expected bond length of 2.04 Å, based on ionic size, but is in reasonable agreement with the average value of 2.0910 Å predicted by the computational model of Arroyo *et al*. [21] for the *Pmnb* structure. This indicates that the manganese tetrahedra are distorted, which is confirmed by the large distribution of O-Mn-O bond angles. This finding is in agreement with the published data for Li_2CdSiO_4 which shows distorted Cd tetrahedra [30].

BVS (Table 1) show that all atoms (with the exception of lithium) are underbonded. In particular, the BVS sum for manganese is 15.5% less than the expected value, which is consistent with the distorted manganese tetrahedra (Table 2). The BVS for the other atoms, although less than the expected values, are within the acceptable range of values considering the approximate nature of BVS calculations.

Complete delithiation of Li_2MnSiO_4 with *Pmnb* symmetry (Fig. 4b) would result in $MnSiO_4$

layers disconnected from each other, causing lattice expansion along the y-direction as a

consequence of the electrostatic repulsion of the oxygen anions in adjacent layers. This

delithiated state is therefore unlikely to occur in practice. It is more likely that delithiation of

Li_2MnSiO_4 with *Pmnb* symmetry would result in a lattice re-arrangement (as demonstrated

for Li_2FeSiO_4) or structural collapse and amorphization (as found for the *Pmn*2_1 polymorph

of Li_2MnSiO_4) [5, 13, 22, 40]. A driver for structural change is the instability of Mn^{3+} and

Mn^{4+} in tetrahedral coordination. Mn^{3+} is typically found in distorted octahedral or square-

pyramidal coordination while Mn^{4+} is usually found in octahedral coordination. This implies

that oxidizing Mn^{2+} while maintaining tetrahedral coordination is likely to be difficult [25].

The presence of Mn^{3+} cations in delithiated Li_2MnSiO_4 may also result in a dynamic Jahn-

Teller distortion of the lattice, which has been shown to be a significant factor in the capacity

fade of other Mn^{3+}-containing cathode materials such as $LiMn_2O_4$ spinels [41].

3.2   *Morphology*

SEM analysis of the material shows that smaller particles are sintered together to form larger,

irregular agglomerates of up to 50 µm, consistent with the relatively high temperature of

synthesis (900 ℃, Fig. 5). Despite the presence of the carbonaceous additive (adipic acid),

the sintering process is not inhibited at this high temperature.

3.3   *Electrochemistry*

Fig. 6 shows the galvanostatic charge and discharge curves for the first cycle for a Li/Li$_2$MnSiO$_4$ (*Pmnb* polymorph) cell at ambient temperature with a current rate of 20 mAg^{-1} and voltage limits of 4.9 and 2.5 V, respectively. The first charge cycle shows a steady increase in voltage with charge and a capacity of 230 mAhg^{-1}, corresponding to the extraction of 1.3 lithium per formula unit. Lithium cannot be re-inserted in large quantities on the subsequent discharge (20 mAhg^{-1}, corresponding to 0.1 lithium per formula unit).

The poor electrochemical performance may be ascribed to two factors. Firstly, it should be noted that the morphology of this sample (Fig.5), prepared by solid state synthesis, is not optimal for electrochemical performance. Large, poorly-conducting particles result in large polarization and it is possible that some of the capacity observed on charge can be attributed to irreversible reactions, for example, electrolyte decomposition, occurring at the high voltages reached and not exclusively to lithium extraction. Since the *Pmnb* polymorph of Li$_2$MnSiO$_4$ can be readily formed in the solid state at 900 °C, alternative synthesis routes e.g. sol-gel or hydrothermal synthesis that typically generate fine particles with a carbon coating, are also expected to yield this polymorph at calcination temperatures above 700 °C. Fine, carbon-coated powders would show reduced polarization on charge enabling the extraction of lithium at lower voltages and preventing unwanted side-reactions. Secondly, it is likely that, as in the case of the *Pmn2$_1$* polymorph, the extraction of lithium during the first charge cycle results in a structural re-arrangement or amorphization of the lattice which limits lithium re-insertion on the subsequent discharge cycle [5, 13, 22].

4. Conclusion

In this study we have prepared the *Pmnb* polymorph of Li$_2$MnSiO$_4$ without significant impurities. Rietveld refinement of a structural model using a combination of high resolution

SXRPD and NPD data shows that the sample is isostructural with Li_2CdSiO_4 with $a = 6.30694(3)$ Å, $b = 10.75355(4)$ Å, and $c = 5.00863(2)$ Å, confirming the previously proposed structure [21, 24]. Bond lengths, angles, and BVS from this model are physically realistic, where the manganese tetrahedra are found to be distorted. Electrochemical results show poor galvanostatic cycling performance. Alternative synthesis routes aimed at improving the electrochemical performance of this polymorph will be explored in future work.

References

[1]   Z.G. Yang, J. Liu, S. Baskaran, C.H. Imhoff, J.D. Holladay, J.O.M. 62 (2010) 14-23.

[2]   T. Xu, W. Wang, M.L. Gordin, D.H. Wang, D.W. Choi, J.O.M. 62 (2010) 24-30.

[3]   A. Manthiram, J. Phys. Chem. 2 (2011) 176-184.

[4]   C. Daniel, J.O.M. 60 (2008) 43-48.

[5]   R. Dominko, J. Power Sources 184 (2008) 462-468.

[6]   R. Dominko, M. Bele, M. Gaberscek, A. Meden, M. Remskar, J. Jamnik, Electrochem. Commun. 8 (2006) 217-222.

[7]   R. Dominko, M. Bele, A. Kokalj, M. Gaberscek, J. Jamnik, J.Power Sources 174 (2007) 457-461.

[8]   C. Lyness, B. Delobel, A.R. Armstrong, P.G. Bruce, Chem. Commun. (2007) 4890-4892.

[9]   A. Nyten, A. Abouimrane, M. Armand, T. Gustafsson, J.O. Thomas, Electrochem. Commun. 7 (2005) 156-160.

[10]   C. Deng, S. Zhang, B.L. Fu, S.Y. Yang, L. Ma, Mater. Chem.Phys. 120 (2010) 14-17.

[11]   I. Belharouak, A. Abouimrane, K. Amine, J. Phys. Chem. C 113 (2009) 20733-20737.

[12]   W.G. Liu, Y.H. Xu, R. Yang, J. Alloys Compds. 480 (2009) L1-L4.

[13]   W.G. Liu, Y.H. Xu, R. Yang, Rare Metals 29 (2010) 511-514.

[14]   W.G. Liu, Y.H. Xu, R. Yang, M. Hojamberdiev, Z.B. Zhou, J. Inorg. Mater. 25 (2010) 327-331.

[15]   V. Srinivasan, J. Newman, J. Electrochem. Soc. 151 (2004) A1517-A1529.

[16]   J.D. Wilcox, M.M. Doeff, M. Marcinek, R. Kostecki, J. Electrochem. Soc. 154 (2007) A389-A395.

[17]   A. Manthiram, T. Muraliganth, K.R. Stroukoff, Chem. Mater. 22 (2010) 5754-5761.

[18]   V. Aravindan, K. Karthikeyan, S. Ravi, S. Amaresh, W.S. Kim, Y.S. Lee, J. Mater. Chem. 20 (2010) 7340-7343.

[19]   K. Karthikeyan, V. Aravindan, S.B. Lee, I.C. Jang, H.H. Lim, G.J. Park, M. Yoshio, Y.S. Lee, J. Power Sources 195 (2010) 3761-3764.

[20]   D. Lv, W. Wen, X. Huang, J. Bai, J. Mi, S. Wu, Y. Yang, J. Mater. Chem. 21 (2011) 9506-9512.

[21]   M.E. Arroyo-DeDompablo, R. Dominko, J.M. Gallardo-Amores, L. Dupont, G. Mali, H. Ehrenberg, J. Jamnik, E. Moran, Chem. Mater. 20 (2008) 5574-5584.

[22]   A. Kokalj, R. Dominko, G. Mali, A. Meden, M. Gaberscek, J. Jamnik, Chem. Mater. 19 (2007) 3633-3640.

[23]   A.R. Armstrong, C. Lyness, M. Menetrier, P.G. Bruce, Chem. Mater. 22 (2010) 1892-1900.

[24]   G. Mali, A. Meden, R. Dominko, Chem. Commun. 46 (2010) 3306-3308.

[25]   V.V. Politaev, A.A. Petrenko, V.B. Nalbandyan, B.S. Medvedev, E.S. Shvetsova, J. Solid State Chem. 180 (2007) 1045-1050.

[26]   K.S. Wallwork, B.J. Kennedy, D. Wang, AIP Conference Proceedings (2007) 879.

[27]   K.D. Liss, B. Hunter, M. Hagen, T. Noakes, S. Kennedy, Physica B 385-86 (2006) 1010-1012.

[28]   A.C. Larson, R.B.V. Dreele, Los Alamos National Laboratory Report LAUR (1994) 86-748.

[29]   B.H. Toby, J. Appl. Crystallogr. 34 (2001) 210-213.

[30]   C. Riekel, Acta Crystallogr. B 33 (1977) 2656-2657.

[31]   N.N. Lobanov, L.A.d. Veiga, Sixth European Powder Diffraction Conference August 22-25 (1998).

[32]   V.F. Sears, Neutron News 3 (1992) 29.

[33]   N. Sharma, R.L. Withers, K.S. Knight, C.D. Ling, J. Solid State Chem. 182 (2009) 2468-2474.

[34]   N. Sharma, R.B. Macquart, M.M. Avdeev, M. Christensen, G.I. McIntyre, Y.-S. Chen, C.D. Ling, Acta Crystallogr. B 66 (2010) 165-172.

[35]   R.J. Gummow, N. Sharma, V.K. Peterson, Y. He, J. Power Sources (2011) doi:10.1016/j.jpowsour.2011.09.013.

[36]   A. Boulineau, C. Sirisopanaporn, R. Dominko, A.R. Armstrong, P.G. Bruce, C. Masquelier, Dalton Trans. 39 (2010) 6310-6316.

[37]   C. Sirisopanaporn, A. Boulineau, D. Hanzel, R. Dominko, B. Budic, A.R. Armstrong, P.G. Bruce, C. Masquelier, Inorg. Chem. 49 (2010) 7446-7451.

[38]   R.D. Shannon and C.T. Prewitt, J. Inorg. Nucl. Chem. 32 (1970) 1427-1441.

[39]   R.D. Shannon, C.T. Prewitt, Acta Crystallogr. B 25 (1969) 925.

[40]   A.R. Armstrong, N. Kuganathan, M.S. Islam, P.G. Bruce, J. Am. Chem. Soc. 133 (2011) 13031-13035.

[41]   R.J. Gummow, A. De Kock, M.M. Thackeray, Solid State Ionics 69 (1994) 59-67.

Table 1

Table 1. Refined crystallographic parameters for Li_2MnSiO_4, space group *Pmnb* using combined SXRPD and NPD data, with a = 6.306938(25) Å, b = 10.75355(4) Å, and c = 5.008629(23) Å, with combined parameters R_p = 2.74%, wR_p = 3.70%, and χ^2 = 1.86, and R_F^2 (NPD) = 9.31%, and R_F^2 (SXRPD) = 8.73% for 45 variables.

Atom	Wyckoff	x	y	z	Site Occupancy Factor	Isotropic Atomic Displacement Parameter ($\times$ 100)/Å^2	Bond Valence Sum
Li(1)	8*d*	0.5077(8)	0.9129(4)	0.3133(10)	1	2.55(10)	1.06
Mn(1)	4*c*	0.25	0.1653(1)	0.1942(2)	1	0.78(1)	1.69
Si(1)	4*c*	0.25	0.3386(1)	0.6790(3)	1	1.39(33)	3.80
O(1)	4*c*	0.25	0.3433(2)	0.3417(4)	1	1.19(5)	1.82
O(2)	8*d*	0.0366(2)	0.0907(1)	0.2848(3)	1	0.78(4)	1.95
O(3)	4*c*	0.25	0.1926(2)	0.7574(4)	1	0.61(5)	1.87

Table 2

Table 2. Selected bond lengths (Å) and bond angles (º) of the *Pmnb* phase of Li_2MnSiO_4.

Bond	Length (Å)	Bond	Length (Å)	Bond	Length (Å)
Li - O(1)	1.950(5)	Mn - O(1)	2.051(2)	Si - O(1)	1.690(2)
Li - O(2)	1.926(4)	Mn - O(2)	2.029(1)	Si - O(2)	1.633(1)
Li - O(2)	2.033(4)	Mn - O(2)	2.029(1)	Si - O(2)	1.633(1)
Li - O(3)	1.936(5)	Mn - O(3)	2.207(2)	Si - O(3)	1.618(2)
Average	1.961(9)	Average	2.079(3)	Average	1.644(3)
Angle	**(º)**	**Angle**	**(º)**	**Angle**	**(º)**
O(1) - Li - O(2)	115.52(26)	O(1) - Mn - O(2)	106.77(4)	O(1) - Si - O(2)	108.08(8)
O(1) - Li - O(2)	105.78(22)	O(1) - Mn - O(2)	106.77(4)	O(1) - Si - O(2)	108.08(8)
O(1) - Li - O(3)	111.10(20)	O(2) - Mn - O(2)	125.97(8)	O(1) - Si - O(3)	105.76(13)
O(2) - Li - O(2)	96.06(21)			O(2) - Si - O(2)	110.89(12)
O(2) - Li - O(3)	119.56(25)			O(2) - Si - O(3)	111.88(7)
O(2) - Li - O(3)	106.14(23)			O(2) - Si - O(3)	111.88(7)

Figure Captions

Figure 1: a) Calculated XRPD pattern for the *Pmn*2_1 polymorph of Li_2MnSiO_4 (vertical lines indicate peak positions) and collected patterns of Li_2MnSiO_4 synthesized at b) 700 ℃ and c) 900 ℃ where reflections marked with (+) are from Li_2SiO_3, (^) are from MnO and (*) are peaks unaccounted for with the *Pmn*2_1 structural model.

Figure 2: The Rietveld refinement plot using the Li_2MnSiO_4 *Pmnb* model and SXRPD data in the (a) $5 \leq 2\theta \leq 40$ ⁰ and (b) $40 \leq 2\theta \leq 80$ ⁰ regions. Data are shown as crosses, the calculated Rietveld model as a line through the data, and the difference between the data and the model as the line below the data. The reflection markers for Li_2MnSiO_4 (lower markers) and MnO (upper markers) are shown as vertical lines.

Figure 3: The Rietveld refinement plot using the Li_2MnSiO_4 *Pmnb* model and NPD data. Data are shown as crosses, the calculated Rietveld model as a line through the data, and the difference between the data and the model as the line below the data. The reflection markers for Li_2MnSiO_4 (lower markers) and MnO (upper markers) are shown as vertical lines.

Figure 4: The crystal structure of (a) the *Pmnb* form of Li_2MnSiO_4 and (b) the hypothetical structure of the fully delithiated $MnSiO_4$ with SiO_4 shown in blue, LiO_4 in green, and MnO_4 in purple. The central ions in the tetrahedra are shown to indicate the tetrahedral orientation. Crystal axes are shown inset at the bottom left and indicate orientation.

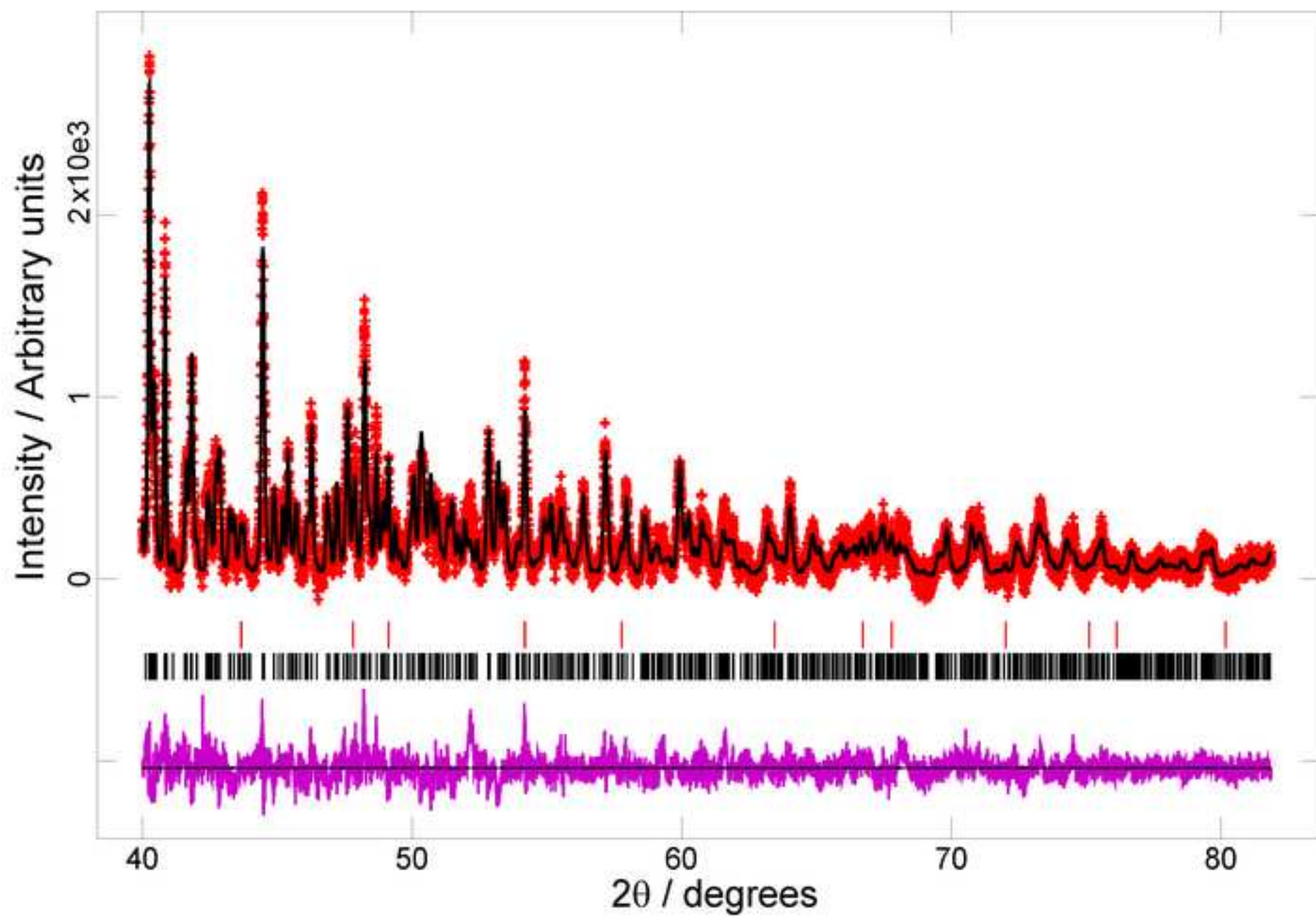**Figure 5**: SEM micrograph of the as-prepared *Pmnb* polymorph of Li_2MnSiO_4.

Figure 6: Galvanostatic cycling curves for the first charge and discharge cycles of a Li/Li$_2$MnSiO$_4$ (*Pmnb* form) cell cycled at a current rate of 20 mA/g between voltage limits of 2.5 and 4.8V.
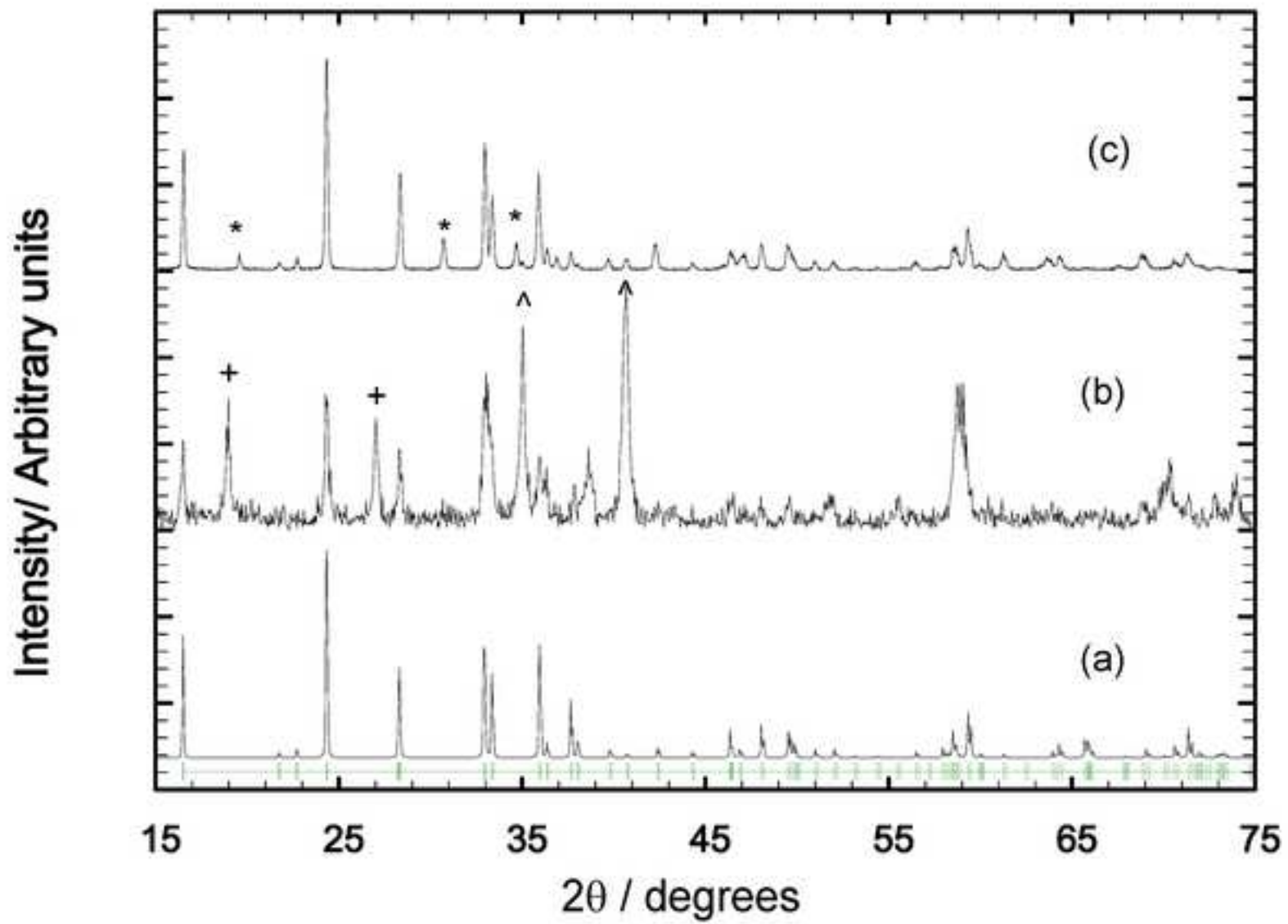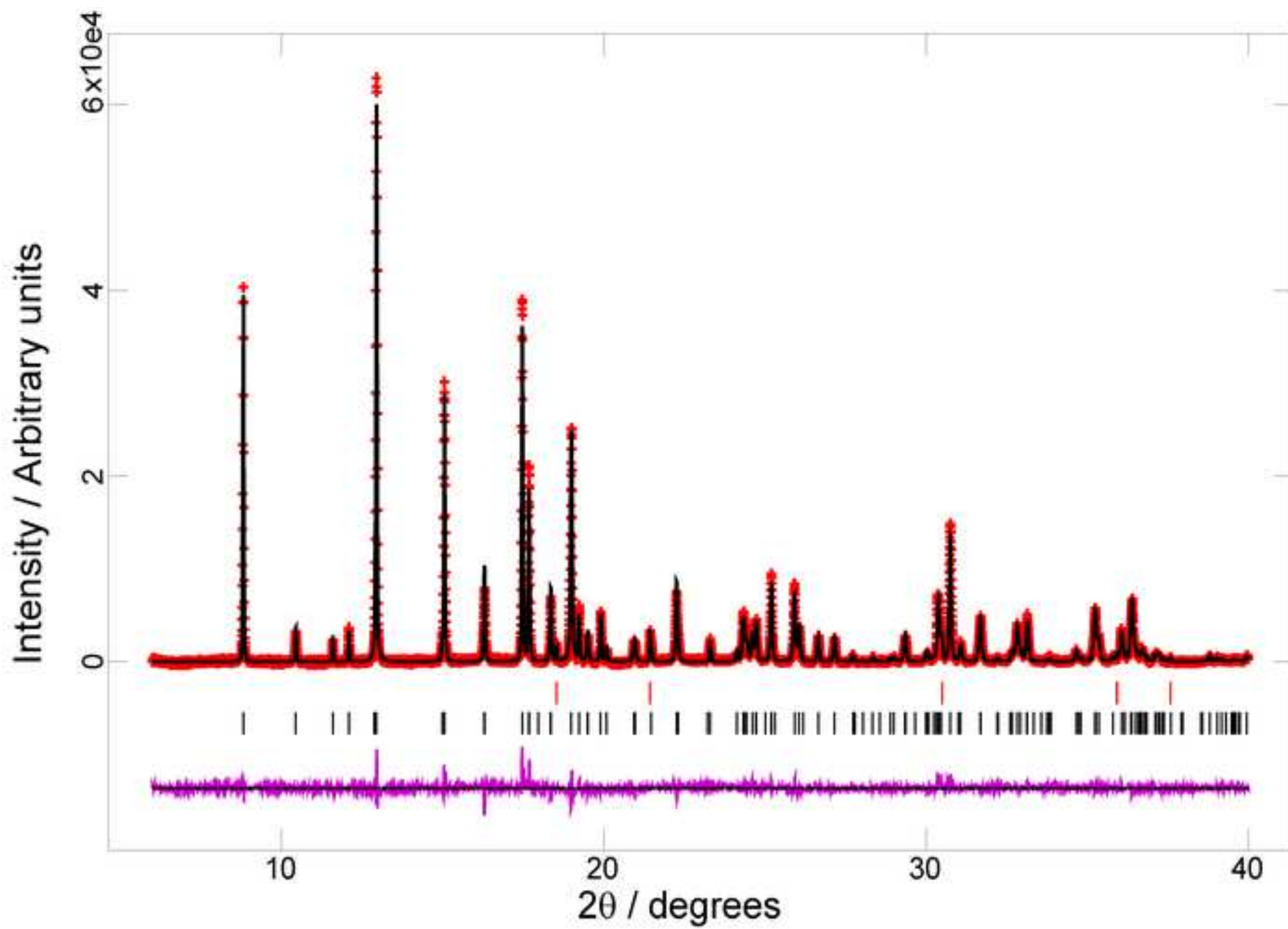
The *Pmnb* form of Li_2MnSiO_4

a, b, c
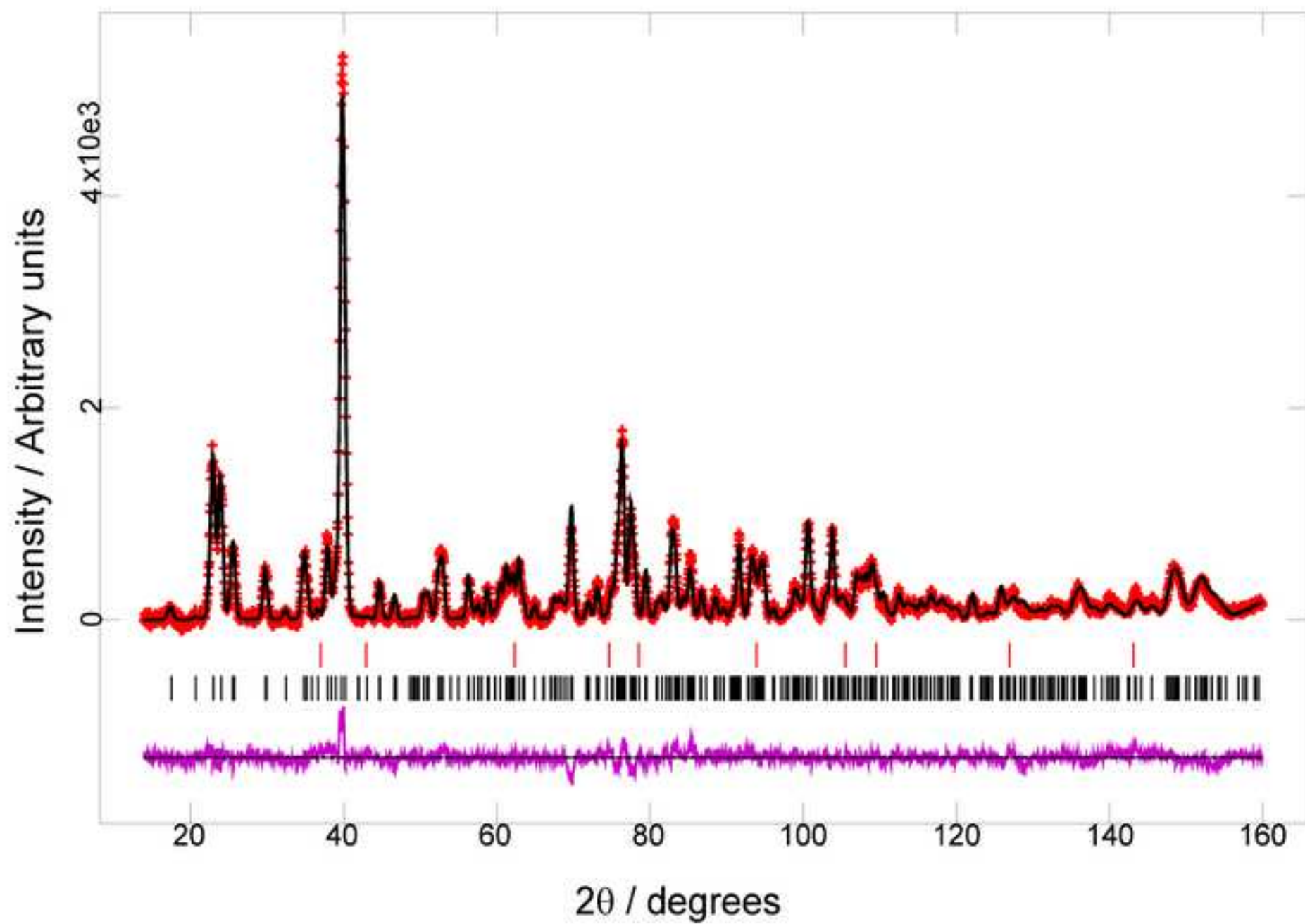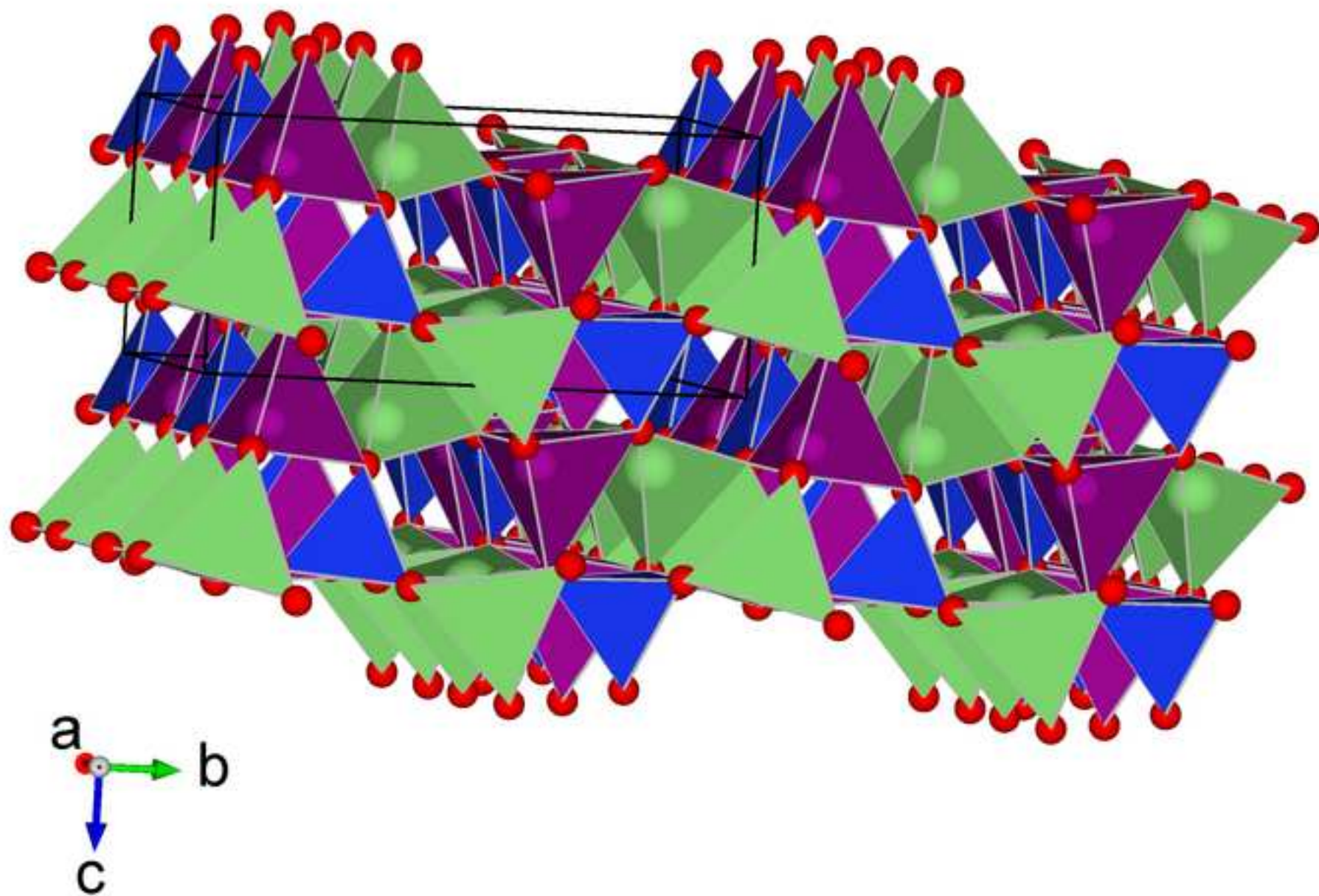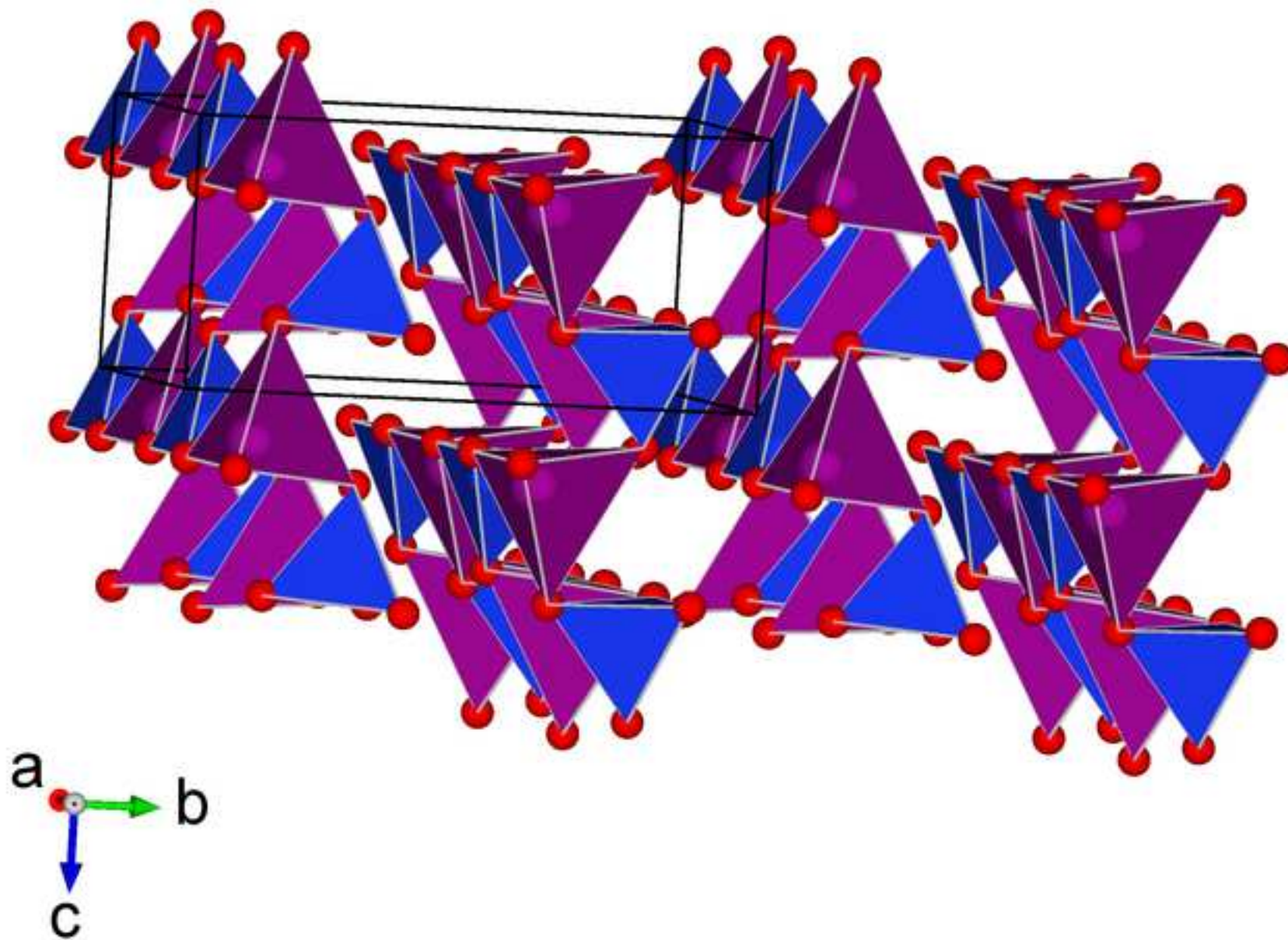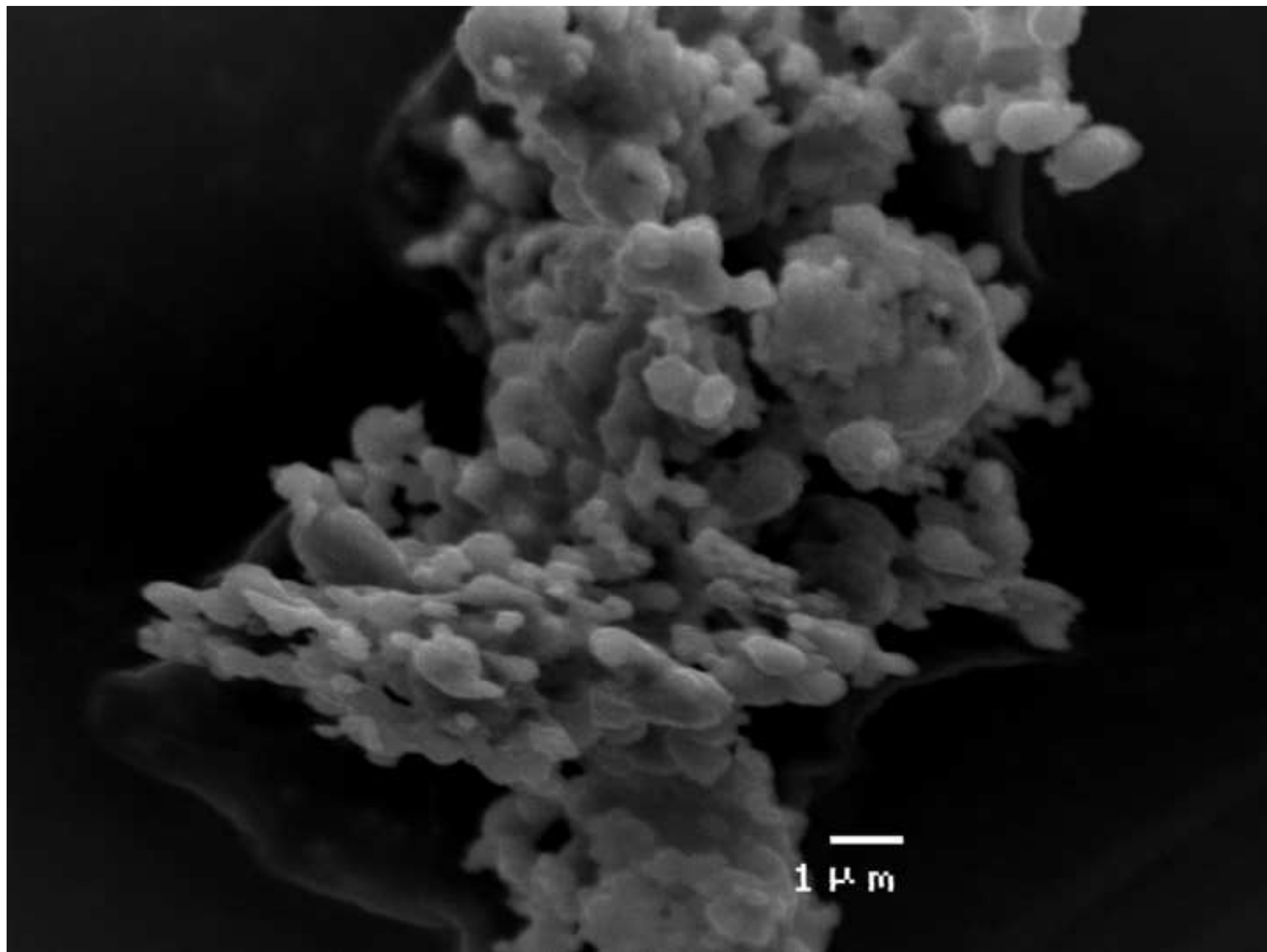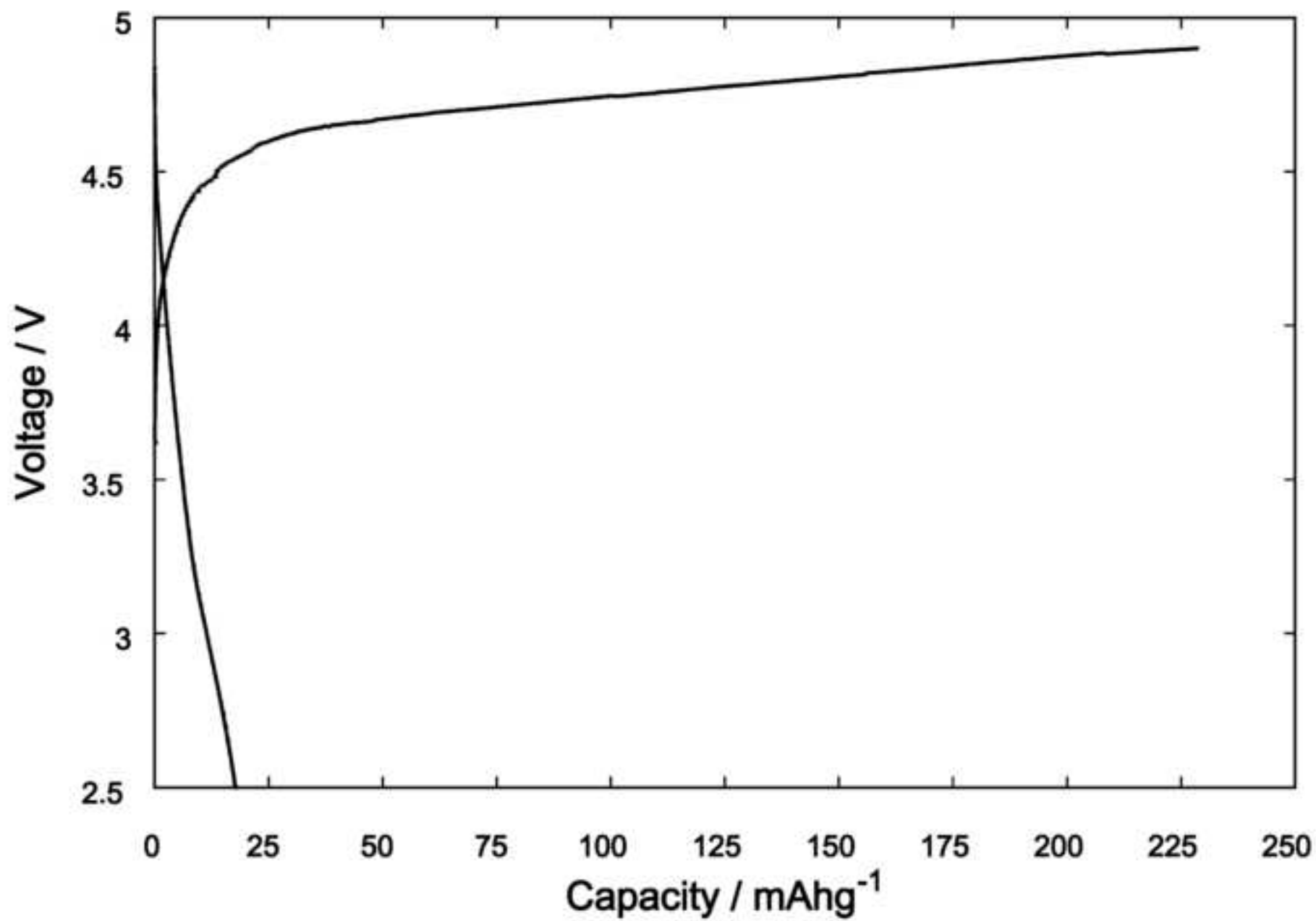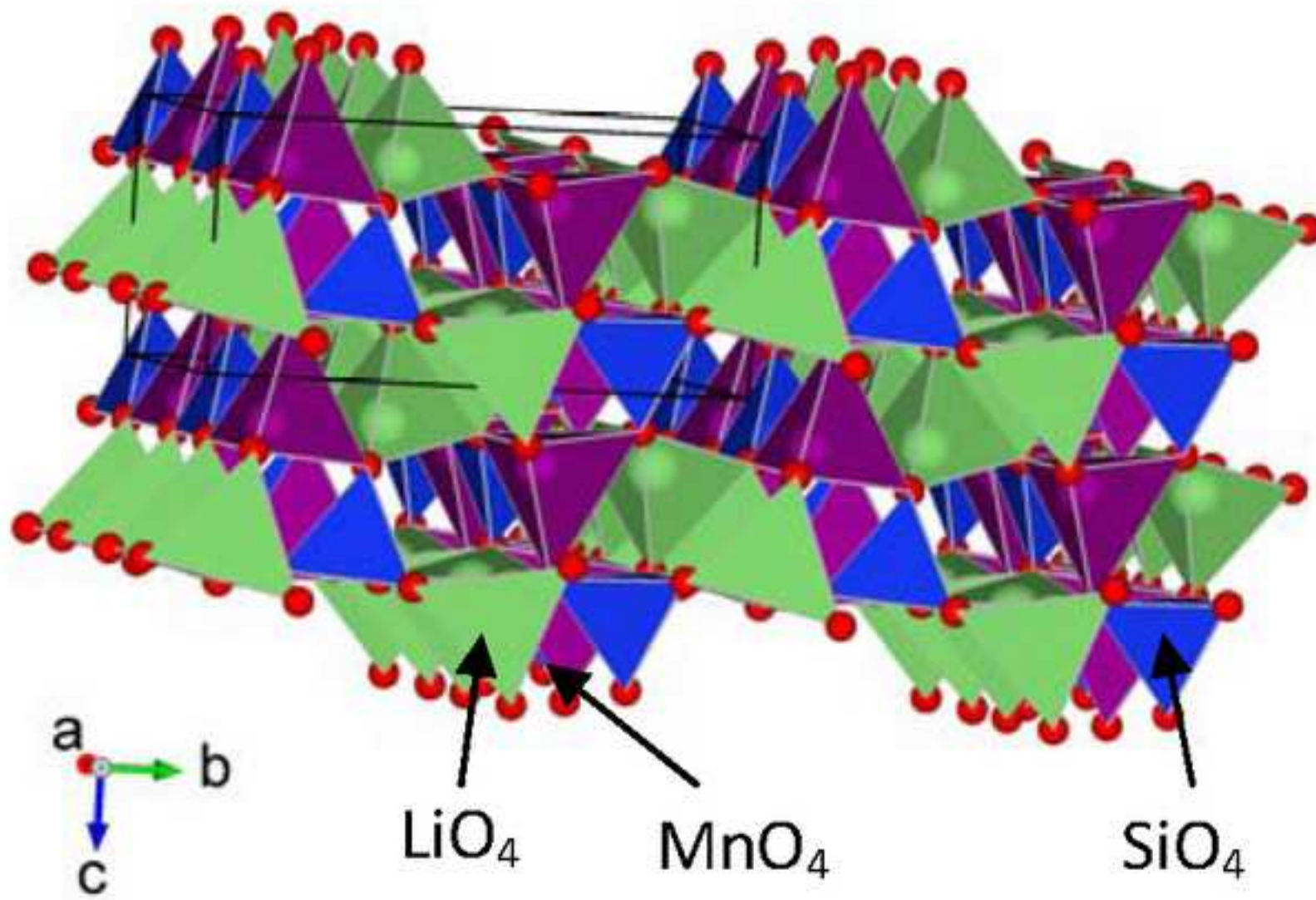
LiO_4 MnO_4 SiO_4

Polyhedral representation of the crystal structure of Li_2MnSiO_4 in the *Pmnb* space group. LiO_4, MnO_4 and SiO_4 tetrahedra are shown in green, purple and blue respectively.

➢ A phase-pure sample of the *Pmnb* polymorph of Li_2MnSiO_4 was synthesized.
➢ Characterized by Rietveld refinement using high resolution synchrotron X-ray and neutron powder diffraction data.
➢ Results confirm the proposed Li_2CdSiO_4-type model with highly distorted Mn tetrahedra.

Supplemental Data

Caption

Click here to download Supplemental Data: Supplementary data Caption.docx

Click here to download Supplemental Data: Supplementary data Caption.docx

Mol Files
Click here to download Mol Files: VESTA_phase_1.mol